



Comparative Assessment of Neutron Flux Sensor Technologies for Advanced Reactors

December 2021

Milestone Report—M3CT-21IN0702014

Kevin Tsai, Michael Reichenberger, and Joe Palmer
Idaho National Laboratory



*INL is a U.S. Department of Energy National Laboratory
operated by Battelle Energy Alliance, LLC*

DISCLAIMER

This information was prepared as an account of work sponsored by an agency of the U.S. Government. Neither the U.S. Government nor any agency thereof, nor any of their employees, makes any warranty, expressed or implied, or assumes any legal liability or responsibility for the accuracy, completeness, or usefulness, of any information, apparatus, product, or process disclosed, or represents that its use would not infringe privately owned rights. References herein to any specific commercial product, process, or service by trade name, trade mark, manufacturer, or otherwise, does not necessarily constitute or imply its endorsement, recommendation, or favoring by the U.S. Government or any agency thereof. The views and opinions of authors expressed herein do not necessarily state or reflect those of the U.S. Government or any agency thereof.

Comparative Assessment of Neutron Flux Sensor Technologies for Advanced Reactors

Milestone report—M3CT-21IN0702014

**Kevin Tsai, Michael Reichenberger, and Joe Palmer
Idaho National Laboratory**

December 2021

**Idaho National Laboratory
Idaho Falls, Idaho 83415**

<http://www.inl.gov>

**Prepared for the
U.S. Department of Energy
Office of Nuclear Energy
Under DOE Idaho Operations Office
Contract DE-AC07-05ID14517**

Page intentionally left blank

ABSTRACT

This report documents the comparative assessment of the rhodium-based self-powered neutron detectors (Rh-SPND), micro-pocket fission detectors (MPFD), and dosimetry wires in heated irradiations at the Neutron Radiography reactor facility at Idaho National Laboratory. The sensors performances are evaluated high-temperature environments (upwards of 850°C) during maximum reactor power to simulate use in advanced reactor applications.

The performance of the Rh-SPNDs indicates the experiment cartridge heater power supply interferes with the SPND signals. This interference become increasingly significant at temperatures above 500°C with minimal interference observed for temperatures below 500°C. This work also demonstrated the fabrication process for the updated design of the MPFD, but issues related to the seal welds were identified and usable data was limited. Finally, the dosimetry measurements were within the expected range correlated with reactor power; thus, the dosimetry results were used to provide preliminary SPND calibration factors.

The results from this experiment serves as a reference for developing and testing of flux sensors that are designed for high-temperature irradiations and advanced reactor deployments. This includes upcoming FY22 irradiations at the Massachusetts Institute of Technology Reactor and the Neutron Radiography (NRAD) reactor utilizing additional fission chambers from Photonis Technologies and fission chambers and SPNDs from The French Alternative Energies and Atomic Energy Commission.

Page intentionally left blank

ACKNOWLEDGEMENTS

The authors would like to thank these people for their significant contributions to the success of this work: Ashley Lambson for the fabrication of the first MPFD new design prototype, Lisa Moore-McAteer for procurement and logistics support for fabrication parts, Randel Paulsen for assembly, testing, and operation of the experiment vehicle, Bryce Kelly for the design and fabrication of the MPFD break-out box, Troy Unruh for design and test procedure consultation, and NRAD Engineering and Operations for experiment deployment and reactor operation.

Page intentionally left blank

CONTENTS

ABSTRACT.....	iii
ACKNOWLEDGEMENTS.....	v
ACRONYMS.....	x
1. INTRODUCTION.....	1
1.1 Sensor Overview	1
1.1.1 Rh-SPND Design and Operation	1
1.1.2 MPFD Design and Operation.....	2
2. METHOD.....	3
2.1 Experiment Setup.....	3
2.2 Operational Procedure.....	4
3. RESULTS AND DISCUSSION	4
3.1 Irradiation #1 (SPND).....	4
3.1.1 Startup and Heating to 800°C (Segment 1/2).....	5
3.1.2 Power Reduction and Temperature Drop (Segment 2/2)	6
3.2 Irradiation #2 (SPNDs and MPFD).....	7
3.2.1 Startup and Heating to 750°C (Segment 1 of 4)	8
3.2.2 Heating to 850°C with DC Power Supply (Segment 2 of 4).....	9
3.2.3 Maintaining 850°C with AC Power Supply (Segment 3 of 4).....	10
3.2.4 Reactor Power Drop without Heater (Segment 4 of 4)	11
3.3 Dosimetry Results	12
4. SUMMARY AND CONCLUSION.....	12
5. REFERENCES.....	13
Appendix A.....	15
Additional Figures from TEV-4296: Heated Instrumentation Rig Assembly	15
Appendix A Additional Figures from TEV-4296: Heated Instrumentation Rig Assembly.....	17

FIGURES

Figure 1. Overview sketch of SPND design.	2
Figure 2. Partial isometric view of MPFD assembly with a single node with item 5 listed as electrode with slot on spacer containing the fissile deposit.	3
Figure 3. Plot of ILC-102-RhSPND signals during reactor startup and heating to 800°C.	5
Figure 4. Plot of ILC-102-RhSPND signals during down-power and temperature-drops.	6
Figure 5. Rh-SPND output during reactor startup and heating to 750°C.	8
Figure 6. Maintaining 750°C and switching heater power supply from AC to DC power supply then heating to 850°C.	9
Figure 7. Maintaining 850°C with AC power supply.	10
Figure 8. Turning off heater power and reducing power.	11
Figure 9. Sideview of NRAD irradiation vehicle.	17
Figure 10. Top-down view of heated irradiation vehicle with sensor position designation numbers.	18
Figure 11. NRAD heated irradiation vehicle orientation and position within the NRAD reactor tank.	19

TABLES

Table 1. Materials and geometry of ILC procured Rh-SPNDs.	2
Table 2. Sensor loadout description for both heated irradiations at NRAD.	4
Table 3. Instrument control and readout configuration.	4
Table 4. Dosimetry measurement results for irradiation #1 and #2.	12
Table 5. Preliminary calibration factors for Rh-SPNDs.	12
Table 6. Guide tube depth for each sensor position.	18

Page intentionally left blank

ACRONYMS

ATR	Advanced Test Reactor
ATRC	Advanced Test Reactor Critical
ILC	Idaho Laboratories Corporation
INL	Idaho National Laboratory
MPFD	micro-pocket fission detector
NRAD	Neutron Radiography
Rh-SPND	Rhodium-based self-powered neutron detector
SPND	self-powered neutron detector
TEV	Technical Evaluation
TREAT	Transient Reactor Test (facility)

Page intentionally left blank

Comparative Assessment of Neutron Flux Sensor Technologies for Advanced Reactors

1. INTRODUCTION

This report documents the heated irradiations of the rhodium-based self-powered neutron detectors (Rh-SPNDs) and the micro-pocket fission detectors (MPFDs) conducted at the Neutron Radiography facility (NRAD) at Idaho National Laboratory (INL). Both technologies are the present focus of development in neutron flux sensors at INL. The primary focus of these experiments is to evaluate the performance of neutron flux sensor technologies operating in high-temperature environments (in excess of 800°C) for advanced reactor application. The two heated irradiations were conducted as a step in establishing a reliable pipeline of neutron flux sensors with a calibration and qualification pathway for commercial adaptation.

The Rh-SPNDs used in these heated irradiations were designed by INL; procured and fabricated from Idaho Laboratories Corporation (ILC). The Rh-SPNDs from these evaluations were previously irradiated in ambient temperatures at the NRAD facility, Advanced Test Reactor Critical (ATRC) facility, and Idaho State University's AGN-201m reactor [1]. The results of these prior irradiations verified proper operation of the SPNDs. The heated experiments at NRAD serve as the basis for analyzing SPND performance and limitations when subjected to a heated environment that is beyond the traditionally observed operational limits for Rh-SPNDs.

Developing in parallel, the MPFDs have also demonstrated successful operation at the Transient Reactor Test (TREAT) facility [2]. The MPFD technology is undergoing a design update with planned irradiations alongside the Rh-SPND at ATRC in support of characterizing test positions to increase utilization efficiency of future deployments at the Advanced Test Reactor (ATR) [3]. Hence, the MPFD used in the NRAD heated irradiation is the first prototype utilizing the updated design with the primary focus on the development of in-house fabrication methods and initial testing of the sensor in a reactor.

Alongside the neutron flux sensors, conventional dosimeter wires utilizing cobalt and nickel were included in both irradiations. Both wire types are commonly used at INL; therefore, the wires are readily available and are well characterized to provide average thermal and fast neutron fluence rate measurements in accordance with American Society for Testing Materials (ASTM) standards E481 and E264. These dosimetry data serve as a baseline for sensor calibration and the development of temperature compensation tools.

1.1 Sensor Overview

1.1.1 Rh-SPND Design and Operation

As previously discussed, the Rh-SPND used in these series of heated irradiations are from the same design of SPNDs from ILC that was evaluated in ambient temperatures. These designs are described in Table 1 and shown Figure 1.

Table 1. Materials and geometry of ILC procured Rh-SPNDs.

SPND Design	Emitter	Insulator at non-sensitive region	Sheath
Large Rh-SPND (ILC-102-RhSPND)	Rhodium 0.032 in. OD 3.50 in. L	Al_2O_3 0.072 in. OD 0.032 in. ID	I-600 0.102 in. OD 0.072 in. ID
Small Rh-SPND (ILC-080-RhSPND)	Rhodium 0.020 in. OD 3.50 in. L	MgO 0.056 in. OD 0.020 in. ID	I-600 0.080 in. OD 0.056 in. ID

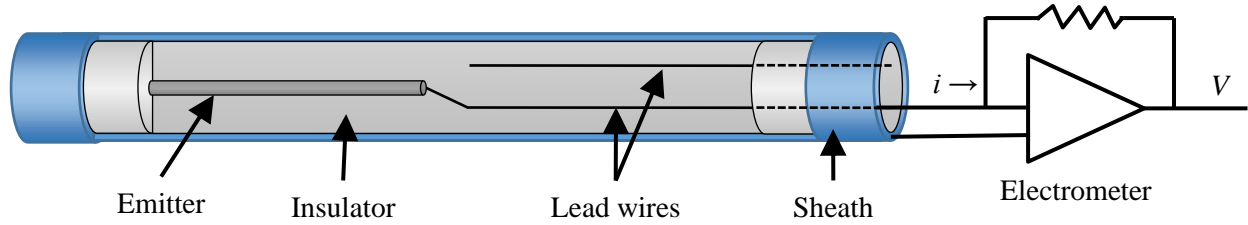


Figure 1. Overview sketch of SPND design.

In operation, the SPNDs generate an electrical current that is linearly proportional to the neutron flux. This is achieved by directly measuring the beta-particles collected at the sheath as a direct result of (n, β^-) reactions in the emitter; as such, SPNDs operate without the need for an external voltage bias. However, the signal time-response is dictated by the decay time constant of the reaction; therefore, Rh-SPNDs are categorized as delayed-response SPNDs. To compensate for the response time, many numerical filters have been designed and may be applied [4]. For simplicity in demonstrating the performance of Rh-SPNDs in high-temperatures, a method of directly solving the decay equation for a compensated signal post-irradiation is used.

$$i_{comp}(t) = \frac{1}{\lambda_B} \frac{di(t)}{dt} + i(t) \quad (1)$$

Where $i(t)$ is the measured signal current of the SPND, $di(t)/dt$ is approximated by the symmetric difference quotient, and λ_B is the activation product decay constant.

1.1.2 MPFD Design and Operation

MPFDs are fission chambers that utilize a very small gas-chamber volume to miniaturize the design for in-core application as well as to provide inherent gamma ray discrimination. The new design also features axially-configurable multi-nodal chambers achieved through stackable mineral insulation disks. As shown in Figure 2, at each designated node location, a spacer exposing two wires is stacked between two disks—one consisting of a small deposit of fissionable materials and the other blank—forming the region necessary for a fission chamber.

The theory of operation of the MPFD mirrors the fission chambers—by measuring the ion currents that are generated from fission fragment ionization within the gas-filled chambers. However, with the design of the MPFD, multiple chambers can be constructed within one continuous cable by utilizing a multi-wire array that contains a central wire to function as a common cathode with adjacent anodes to be terminated at each node [5] [6]. The functionality of this design has been assessed as a part of the planned ATRC irradiation [3]. However, for the purpose of demonstrating the fabrication process and initial testing, the prototype presented in this report will only utilize a single fissile chamber.

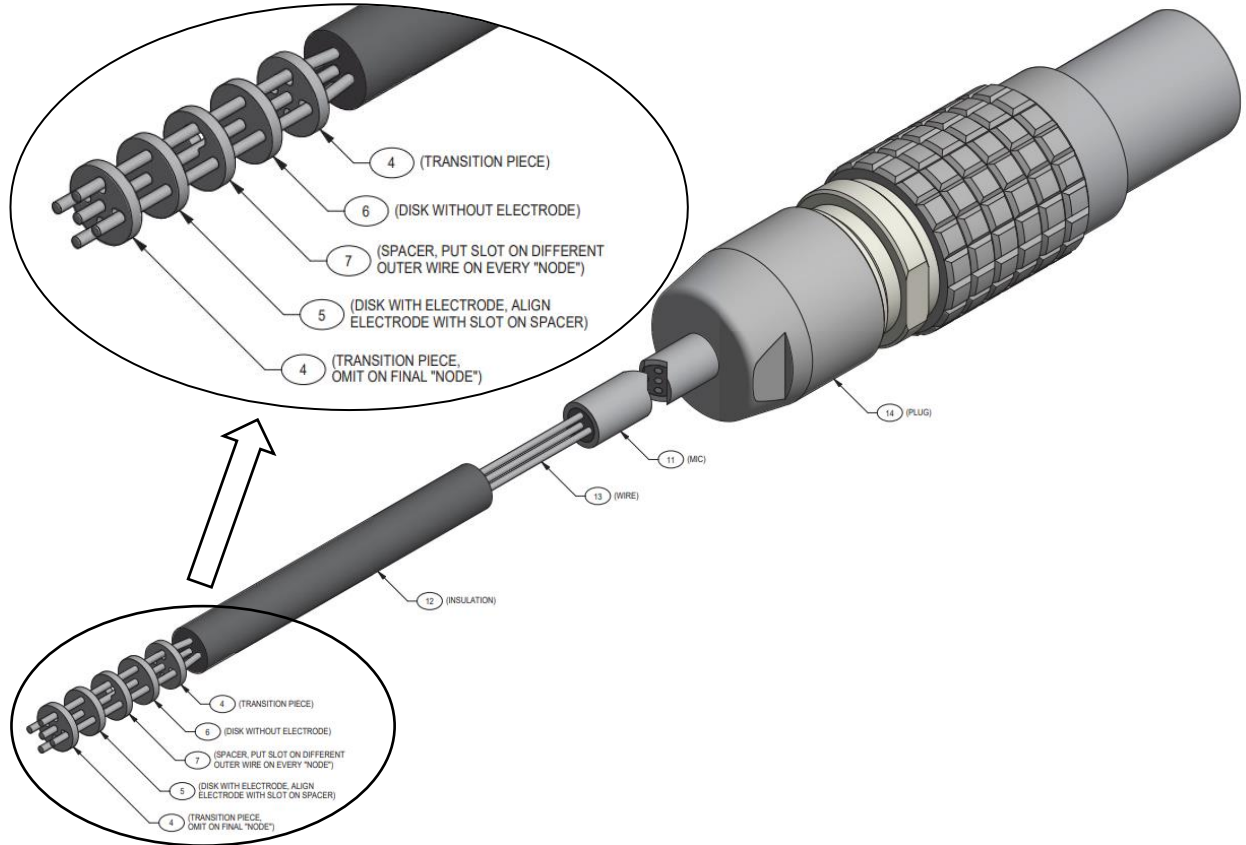


Figure 2. Partial isometric view of MPFD assembly with a single node with item 5 listed as electrode with slot on spacer containing the fissile deposit.

2. METHOD

Two heated irradiations containing the Rh-SPND, MPFD, and dosimeter wires were conducted at the NRAD facility. The following subsections describe the experiment vehicle and procedure.

2.1 Experiment Setup

The irradiation vehicle is comprised of an open-top 2-in. diameter aluminum tube filled with a high-performance insulation and a central heated sensor bundle. The heated sensor bundle consists of six 0.25-in. diameter stainless-steel tubes surrounding a cartridge heater. The stainless-steel tubes function as guide tubes to facilitate sensor insertion and axial positioning with respect to the NRAD reactor core. Sensor positions within the guide tube are given in Table 2. Additional figures and tables describing the vehicle including orientation, position designations, and sensor positions are found in Appendix A and are further documented in Technical Evaluation-4296 (TEV-4296) [7].

The sensors and associated heaters are controlled through independent electronic systems given in

Table 3. Due to the customized requirements of instrument interfacing, each system operates independent of each other. The systems are set to provide timestamped measurements based on the instrument clock; therefore, prior to the start of operation, the clocks of each instrument are synchronized so that data can be easily correlated.

Table 2. Sensor loadout description for both heated irradiations at NRAD.

Position	Irradiation #1 (Performed 8/26/2021) Sensor (Description)	Irradiation #2 (Performed 10/27/2021) Sensor (Description)
1	Type K 3-point thermocouple	MPFD
2	RML Dosimetry (NRAD-1)	RML Dosimetry (NRAD-3)
3	Empty	ILC-Rh-SPND (0.102" OD)
4	Empty	Empty
5	ILC-Rh-SPND (0.102" OD) RML Dosimetry (NRAD-2)	Type K 3-point thermocouple RML Dosimetry (NRAD-4)
6	ILC-Rh-SPND (0.080" OD)	ILC-Rh-SPND (0.080" OD)

Table 3. Instrument control and readout configuration.

Instrument	Electronics	Interface
Heater	Staco Energy 3PN1510B (AC power) B&K Precision 1685B (DC power)*	Manual front panel controls
SPNDs	Keithley 6517B/Keithley 6521	Python
MPFD	Mesytec MPFD-4	LabVIEW
Thermocouples	National Instruments 9214	LabVIEW

* Incorporated on second irradiation only.

2.2 Operational Procedure

The primary objective of the heated irradiation at NRAD is to evaluate sensor performance at pre-designated temperatures. To achieve this objective, the reactor was brought to the maximum operational power of 250 kW and was sustained as temperatures were varied. The designated temperatures for the first irradiation were: 350°C, 500°C, 650°C, and 800°C. The designated temperatures for the second irradiation were: 350°C, 550°C, 750°C, and 850°C. At each designated temperature, the heater output was adjusted to maintain the temperature for a minimum of 30 minutes before ramping to the next designated temperature.

From the first heated irradiation, it was identified that there was potential electronic interference within the experiment vehicle at each heating portion of the experiment which was correlated with the power of the AC power supply. Therefore, a DC power supply was incorporated in the second experiment during the heating from 750°C to 850°C—a region where significant interference was measured during the first experiment.

Once the experiment has attained maximum temperature stabilized for a least 30 minutes, reactor power was decreased to assess sensor response to changing neutron flux at temperature.

3. RESULTS AND DISCUSSION

3.1 Irradiation #1 (SPND)

For the first irradiation, only the Rh-SPNDs were irradiated alongside dosimeter wires (no MPFD). However, the dedicated ILC-080-RhSPND was damaged during assembly at the NRAD facility. Additionally, the reactor power log was deleted due to post-experiment work performed on the reactor console. With the two factors listed, the following two subsections will present on the behavior of the ILC-102-Rh-SPND during (1) heating to maximum temperature of 800°C and (2) reactor down-powering and temperature decrease.

3.1.1 Startup and Heating to 800°C (Segment 1/2)

During the reactor startup and power increase to 250 kW, both signals from the SPND emitter and compensator increased to their expected signal levels as shown in the plots of Figure 3 shortly after the 0-minute timestamp. Additionally, it was observed that the natural heating of the experiment due to reactor power increased the temperature from ambient to 100°C with no observable effect on the SPND signal.

For the emitter signal, a small perturbation was observed during temperature ramps to 350°C with increasingly significant signal drops and subsequent recovery during temperature ramps to 500°C and 650°C. The points of recovery are highly correlated to the timing of the reduction of heater power. However, the observed behavior of signal response did not repeat during the final heat ramp from 650°C to 800°C. The signal had instead undergone a large swing through the duration of heating.

The SPND signal behavior observed indicates a signal deviation induced in the SPND as a result from the heater power input. Additionally, the magnitude of influence from the heater power is correlated to the temperature of the SPND. This effect is only tied to the emitter response. The compensation wire response only demonstrated a strong negative correlation to temperature and not heater power.

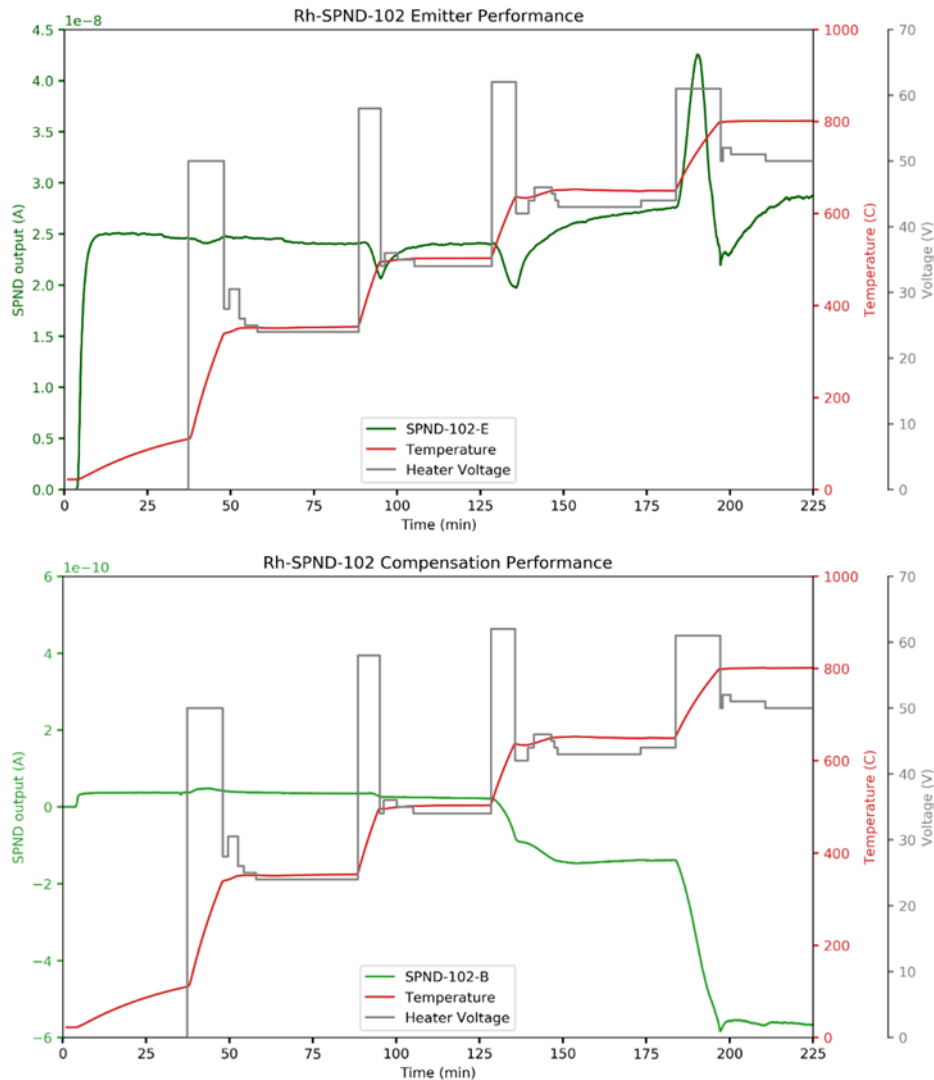


Figure 3. Plot of ILC-102-RhSPND signals during reactor startup and heating to 800°C. (upper) Signals from the emitter and (lower) from the compensation lead wire.

3.1.2 Power Reduction and Temperature Drop (Segment 2/2)

After stabilizing at 800°C, the reactor power was reduced to 200 kW to verify SPND flux tracking at temperature. This occurs at the 230-minute timestamp as the SPND emitter signal drops by the same percentage as reactor power. Remaining at 200 kW, the temperatures are then dropped to 650°C and subsequently 500°C by reducing heater power. Like the segments of the test where the temperature was increased, the compensation wire response continues to demonstrate the strong negative correlation to temperature.

However, the effects on the SPND emitter demonstrated a diminished effect during each temperature changes compared to the heating-up portion of the test. A diminished signal swing in the reduction from 800°C to 650°C was observed. Additionally, the signal drop that was first observed during the temperature change between 500°C and 650°C is significantly reduced during the cooling phase. The final reading of the SPND emitter was 1.9E-8 A at 500°C; compared to the start at ambient temperature of 2.5E-8 A. This indicates a 24% drop in power compared to the 20% drop desired of the reactor—from 250 kW to 200 kW.

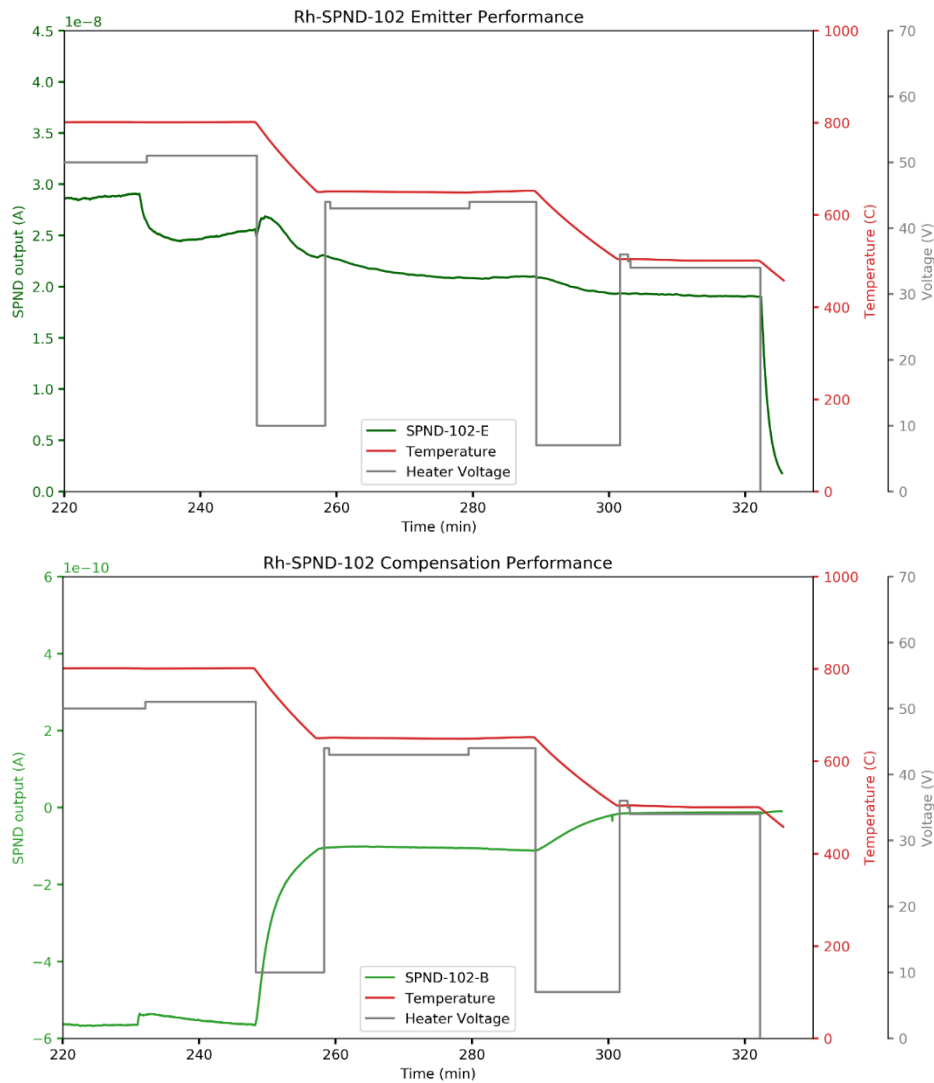


Figure 4. Plot of ILC-102-RhSPND signals during down-power and temperature-drops. (upper) Signals from the emitter and (lower) from the compensation lead wire.

3.2 Irradiation #2 (SPNDs and MPFD)

Following the results of the first heated irradiation, the broken ILC-080-RhSPND was replaced with a spare of the same design. The first prototype of the MPFD was included in the irradiation. Additionally, the heater AC power supply voltage output limit was lowered from 60V to 50V (except the heat-up to 850°C where 60V was required to attain the desired temperature) in an attempt to reduce interference effects that had been previously observed in the first heated irradiation. A second heater power supply utilizing DC output was also incorporated to evaluate the impacts of the power supply's AC characteristics. The four following subsections focus on the following:

1. Reactor startup and heating to 750°C using the AC power supply.
2. Maintaining reactor power and switching to DC power supply and heating to 850°C.
3. Maintaining reactor power and switching back to AC power supply at 850°C.
4. Shutting off the heater and reactor down-power.

During the experiment, it was identified that the MPFD was inoperable. It is suspected that the sensor malfunction was due to a small leak in the chamber. The leak rate was measured during the fabrication process was considered an acceptable leak rate. However, it is assumed that the increased temperature during the experiment made the leak become more significant and rendered the sensor inoperable. Therefore, the following subsections will not include information on the performance of the MPFD and will only detail the performance of the SPND with the attempt to reduce influence from the AC power supply that is used for the heater in the experiment.

3.2.1 Startup and Heating to 750°C (Segment 1 of 4)

In the first segment, the maximum voltage from the AC power supply for heating the experiment vehicle was reduced from 60V (from the first experiment) to 50V. This reduction to the power supply eliminated the phenomena observed in the first irradiation for heating ramps to 350°C and 500°C. The final heating ramp to 850°C, the pulse effect reappeared for the ILC-102-RhSPND, but a negative pulse for the ILC-080-RhSPND was measured. This reinforces the observation that the AC power supply has an increased influence on SPND signals with increasing temperature. An unpredictable pattern has also occurred to the compensation signals. The physical mechanisms that cause these behaviors have yet to be determined.

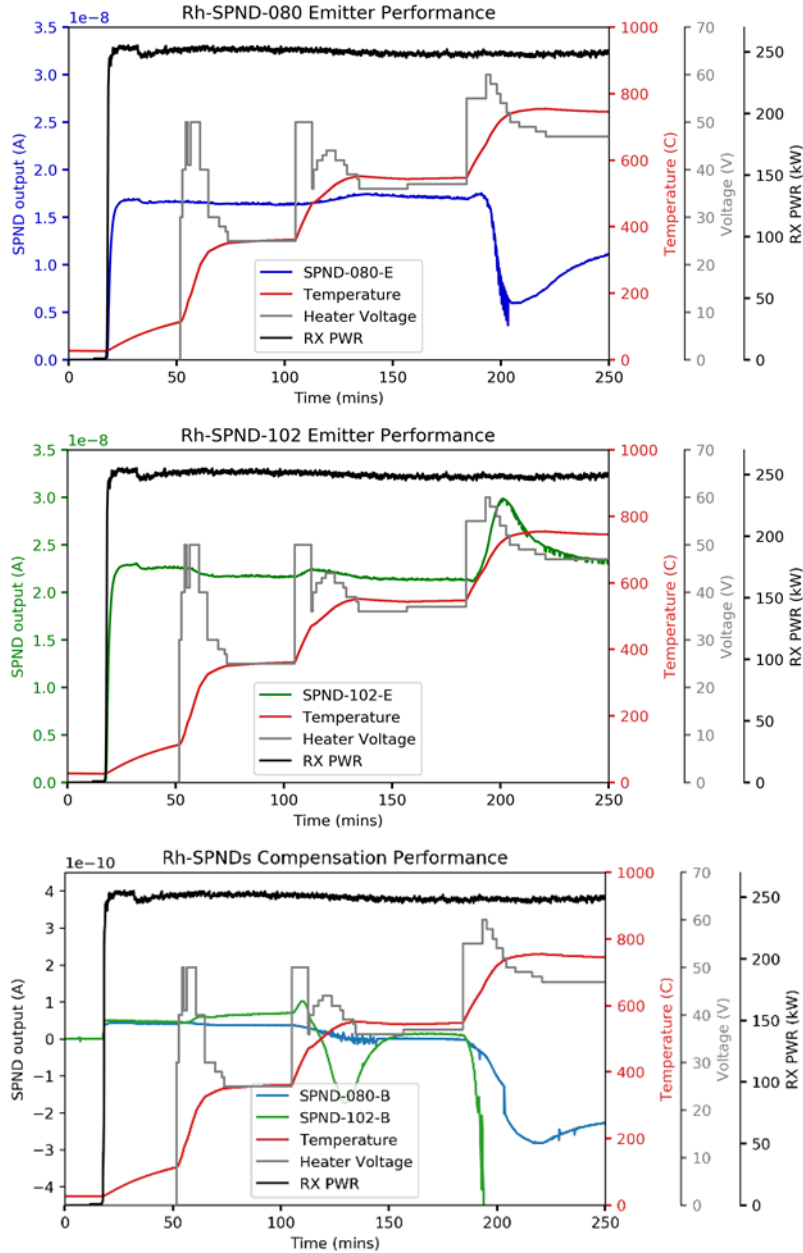


Figure 5. Rh-SPND output during reactor startup and heating to 750°C. (top) SPND-080 emitter signal (middle) SPND-102 emitter signal (bottom) compensation wires from both SPNDs.

3.2.2 Heating to 850°C with DC Power Supply (Segment 2 of 4)

After attaining 750°C, the AC power supply was swapped with a DC power supply as indicated by a drop in heater power near the 260-minute timestamp. After switching the power supply, the DC heater power was applied to maintain the temperature at 750°C. While maintaining 750°C with the DC power supply, the signals were observed to slowly drift down with increased electronic noise as shown by the ILC-080-RhSPND. During the heating to 850°C with the DC power supply, signals from all SPND outputs dropped significantly. This final test verified that the main contribution of signal deviations is derived from the power supply with the DC power supply creating a more significant effect than the AC power supply.

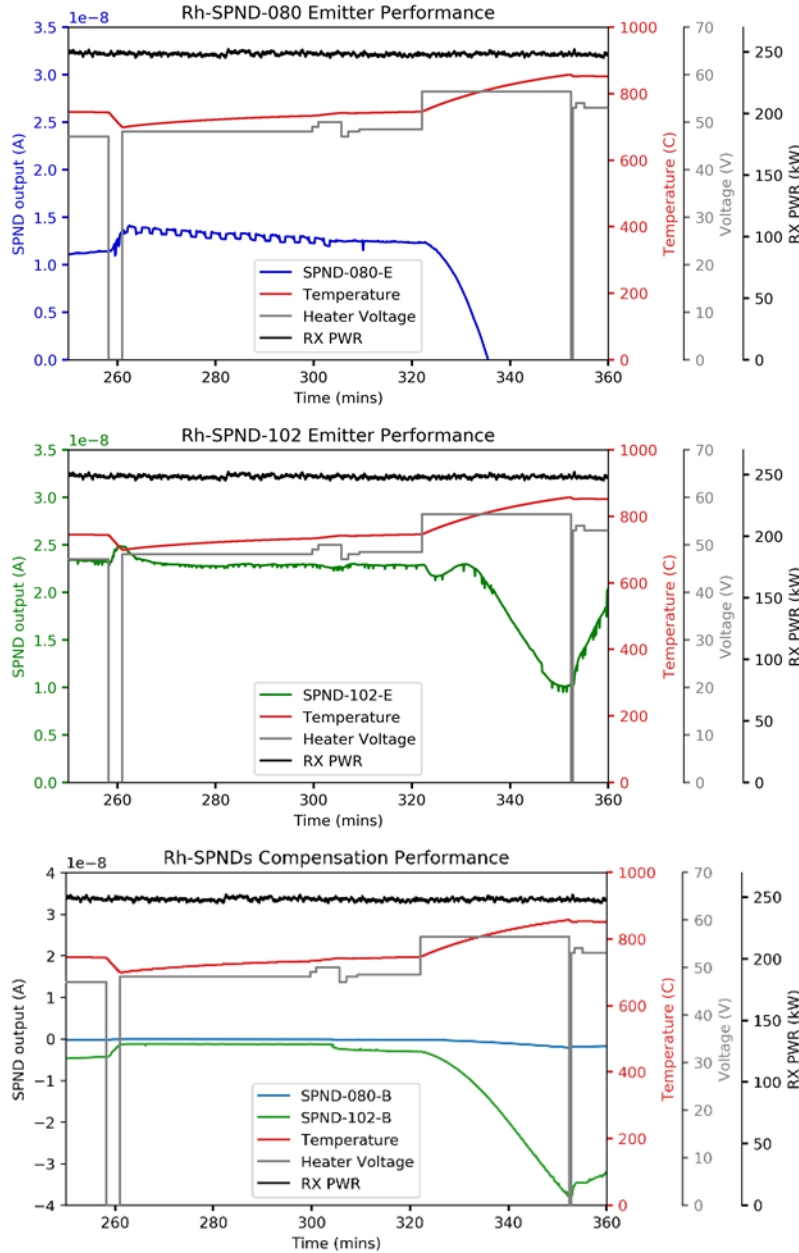


Figure 6. Maintaining 750°C and switching heater power supply from AC to DC power supply then heating to 850°C. (top) SPND-080 emitter signal (middle) SPND-102 emitter signal (bottom) compensation wires from both SPNDs.

3.2.3 Maintaining 850°C with AC Power Supply (Segment 3 of 4)

The heater power supply was swapped back from DC power supply to AC power supply to determine if the loss of signal is caused by the DC power supply could be recovered. The AC heater power supply was operated to maintain the temperature at 850°C, and it was observed that all signals slowly recovered. The recovery observed after switching back to the AC power supply was expected based on the observation made in the previous segment, however, the slow speed of recovery does also suggest that the AC power supply also creates some resistance to signal recovery. This theory is further demonstrated in the next segment.

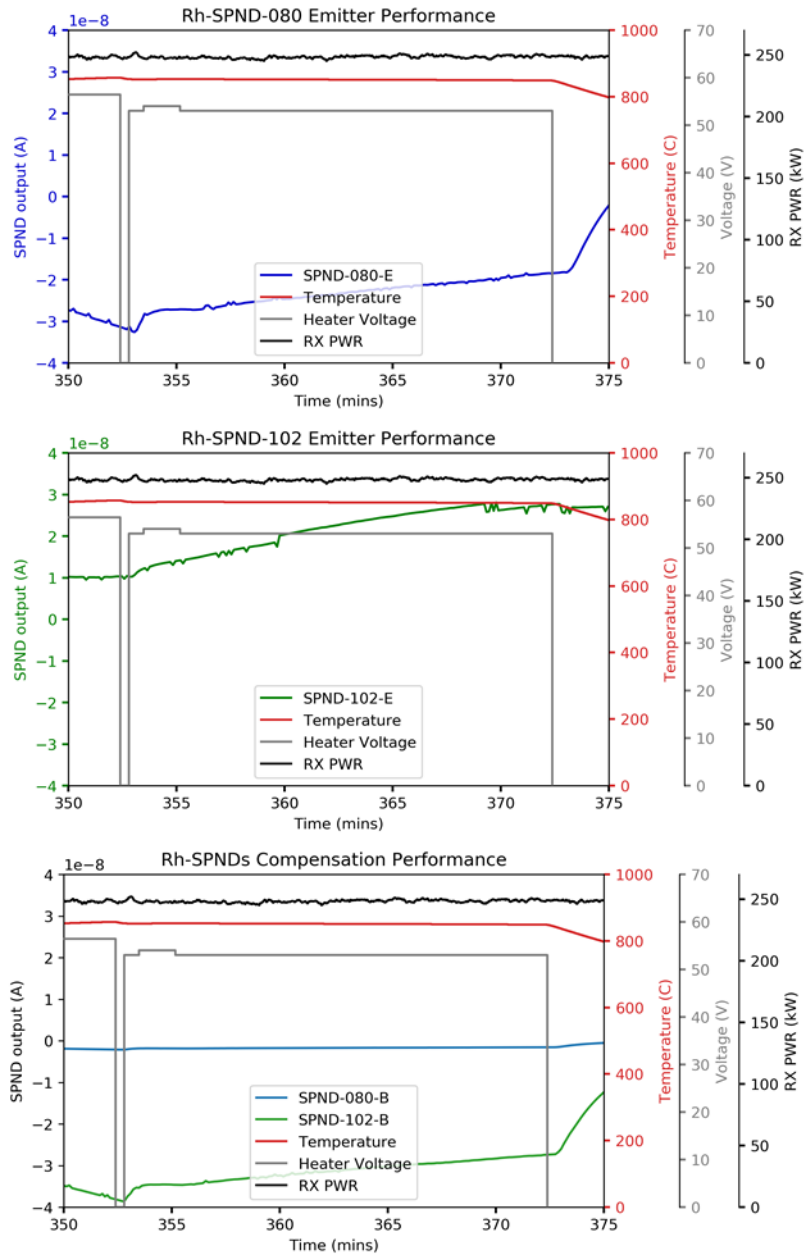


Figure 7. Maintaining 850°C with AC power supply. (top) SPND-080 emitter signal (middle) SPND-102 emitter signal (bottom) compensation wires from both SPNDs.

3.2.4 Reactor Power Drop without Heater (Segment 4 of 4)

For the final segment, the AC heater power supply was turned-off. Afterwards, the SPNDs demonstrated an increased rate of signal output recovery to a level that matched the expected signal at 250 kW reactor power. However, due to the time required for signal to reach expected levels at 250 kW, the temperature had dropped to 400°C. At this point, the reactor operators were directed to reduce power to 25 kW, then 2.5 kW to measure signal response at temperature without heater power supply interference. During the temperature drop from 400°C to 200°C, the Rh-SPNDs demonstrated a highly characteristic signal response to reactor down-power.

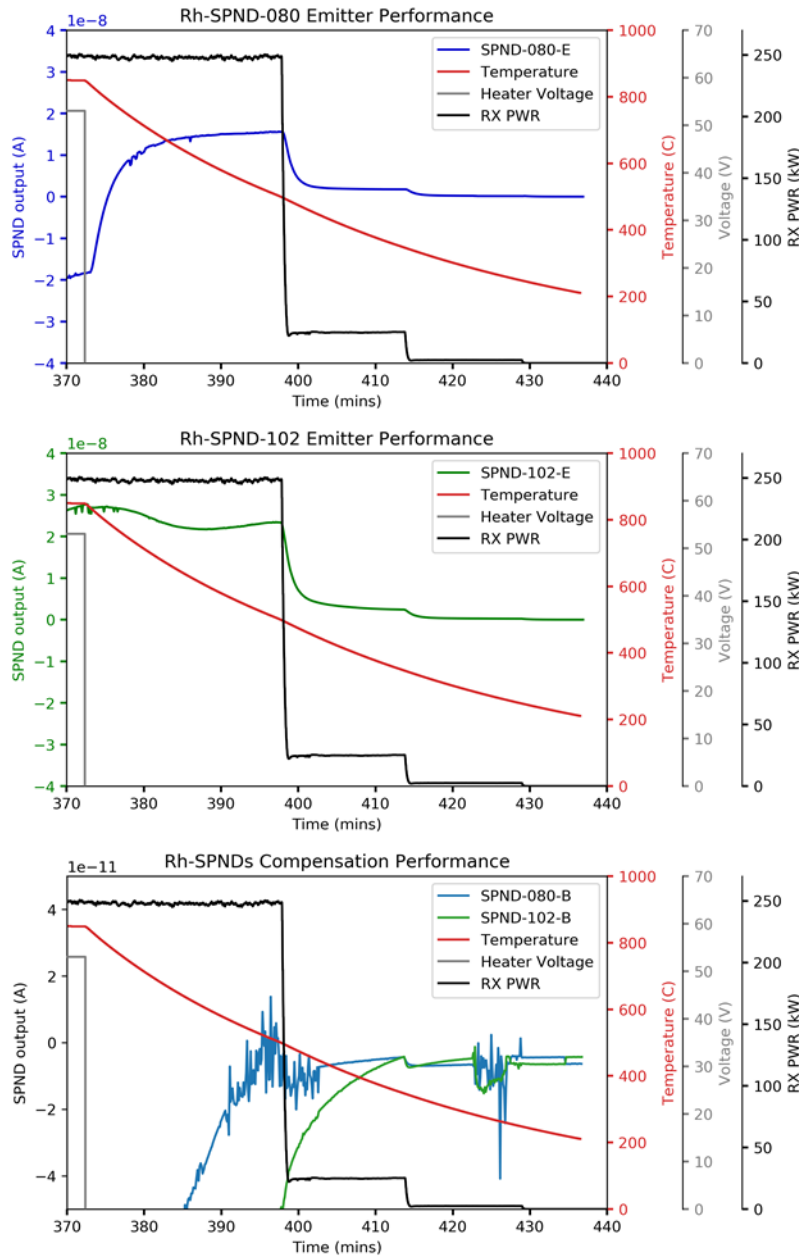


Figure 8. Turning off heater power and reducing power. (top) SPND-080 emitter signal (middle) SPND-102 emitter signal (bottom) compensation wires from both SPNDs.

3.3 Dosimetry Results

The two irradiations varied by average reactor power and irradiation time. While the reactor power data log was unavailable for the first irradiation, it was noted that the reactor was operated at approximately 250 kW for 226.2 minutes and 200 kW for 90.3 minutes—an estimated average power of 235.7 kW for 316.5 minutes. For the second irradiation, the reactor was operated at approximately 250 kW for 378.8 minutes, 25 kW for 16.1 minutes, and 2.5 kW for 16.2 minutes—more accurately calculated directly from the reactor log to result in an average power of 231.5 kW for 411.0 minutes.

Thermal and fast neutron fluence rate measurements provided by the dosimetry wires are given in Table 4. The calculation assumes a steady-state average power over the total duration of irradiation. The assumptions listed above contribute to a small bias of the reported result that is not quantifiable; therefore, only the counting uncertainty is presented. However, despite the expected bias, the percentage increase in thermal and fast neutron fluence rate calculated between the first and second irradiation was -3.73% and -8.88% . This decrease of calculated average fluence rate is near the approximated average power decrease between the two irradiations—235.7 kW for the first irradiation and 231.5 kW for the second irradiation—an estimated -1.78% decrease in reactor power.

Given the availability of data for irradiation #2, the thermal fluence rate calculated from the dosimeter wires ($1.22 \text{ E}+12 \text{ n/cm}^2/\text{s}$ at average reactor power of 231.5 kW) was therefore used to provide a preliminary calibration factor for the Rh-SPNDs—a thermal neutron flux sensor—in this experiment configuration. The calculated SPND sensitivity (given in Table 5) assumes the linearity of the flux with reactor power and is therefore scaled to the Rh-SPND signal at 250 kW prior to heater power supply interference.

Table 4. Dosimetry measurement results for irradiation #1 and #2.

	Irradiation #1		Irradiation #2	
	Calculated	Counting Uncertainty	Calculated	Counting Uncertainty
Thermal fluence rate ($\text{n/cm}^2/\text{s}$)	$1.26\text{E}+12$	$6.30\text{E}+10$	$1.22\text{E}+12$	$6.10\text{E}+10$
Fast fluence rate ($\text{n/cm}^2/\text{s}$)	$2.60\text{E}+11$	$1.30\text{E}+10$	$2.38\text{E}+11$	$1.19\text{E}+10$

Table 5. Preliminary calibration factors for Rh-SPNDs.

SPND Design	Sensitivity ($\text{A}/\phi_{\text{thermal}}$)
ILC-102-RhSPND	$1.71\text{E}-20$
ILC-080-RhSPND	$1.26\text{E}-20$

4. SUMMARY AND CONCLUSION

Two heated irradiations were performed at the NRAD reactor for comparative assessment of neutron sensor technologies for advanced reactors. The sensors deployed within the experiment for evaluation are the Rh-SPNDs, MPFDs, and dosimetry.

The performance of the Rh-SPNDs indicate interference caused by the experiment vehicle's cartridge heater and power supply. The magnitude of interference is observed to be positively correlated to temperature. However, due to the interference magnitude correlation with temperature, it was observed that the Rh-SPNDs were still capable of operating with little to no interference from the cartridge heater and AC power supply used in this experiment at temperatures up to 500°C . Additionally, given the SPND signal recovery even when operating with the AC power supply, it is postulated that future heated irradiations to measure temperature effects are still plausible, but additional irradiation time needs to be included to allow signal stability at each designated temperature above 500°C . To completely avoid the

interference, a new experimental design, utilizing other heating mechanisms such as a heated gas-flowing system would need to be proposed.

This work also served as a platform to demonstrate the prototype fabrication of the MPFD. The issue identified during fabrication lies heavily on the welding capabilities available to seal the chamber sections of the MPFD. The solution is presently being pursued to provide another prototype for future irradiation plans.

While the sensor performances were largely affected due to the experimental setup, the dosimetry measurements still demonstrated its reliability in providing a good baseline fluence rate measurement that was within the expected magnitude despite the high-temperature aspect of the experiment.

The results from this experiment will serve as a reference for improving future evaluations of sensor performance in high-temperature irradiations. This includes upcoming FY22 irradiations at the Massachusetts Institute of Technology Reactor and the NRAD reactor utilizing additional sensors from Photonis Technologies and The French Alternative Energies and Atomic Energy Commission.

5. REFERENCES

6. Bibliography

- [1] INL/EXT-21-62961, "Performance Demonstration of Self-Powered Neutron Detectors for Steady-State Reactor Operations," 2021.
- [2] INL/EXT-18-51613, "FY18 Report for Instrumentation Development for the Transient Testing Program," 2018.
- [3] D. M. Nichols, M. A. Reichenberger, A. D. Maile, M. R. Holtz and D. S. McGregor, "Simulated Performance of the Micro-Pocket Fission Detector in the Advanced Test Reactor Critical Facility," *Nuclear Science and Engineering*, vol. 195, no. 10, pp. 1098-1106, 2021.
- [4] A. K. Mishra, S. R. Shimjith, T. U. Bhatt and A. P. Tiwari, "Kalman Filter-Based Dynamic Compensator for Vanadium Self Powered Neutron Detectors," *IEEE Transactions on Nuclear Science*, vol. 61, no. 3, pp. 1360-1368, 2014.
- [5] M. A. Reichenberger, D. M. Nichols, S. R. Stevenson, T. M. Swope, C. W. Hilger, T. C. Unruh, D. S. McGregor and J. A. Roberts, "Fabrication and testing of a 4-node micro-pocket fission detector array for the Kansas State University TRIGA Mk. II research nuclear reactor," *Nuclear Instruments and Methods in Physics Research A*, vol. 862, pp. 8-17, 2017.
- [6] M. A. Reichenberger, D. M. Nichols, S. R. Stevenson, T. M. Swope, C. W. Hilger, R. G. Fronk, J. A. Geuther and D. S. McGregor, "Fabrication and testing of a 5-node micro-pocket fission detector array for real-time, spatial, iron-wire port neutron-flux monitoring," *Annals of Nuclear Energy*, vol. 110, pp. 995-1001, 2017.
- [7] TEV-4296, "Technical Evaluation: Assembly and Functional Test of NRAD Heated Instrumentation Rig, Rev. 1," 2021.

Page intentionally left blank

Appendix A

Additional Figures from TEV-4296: Heated Instrumentation Rig Assembly

Page intentionally left blank

Appendix A

Additional Figures from TEV-4296: Heated Instrumentation Rig Assembly

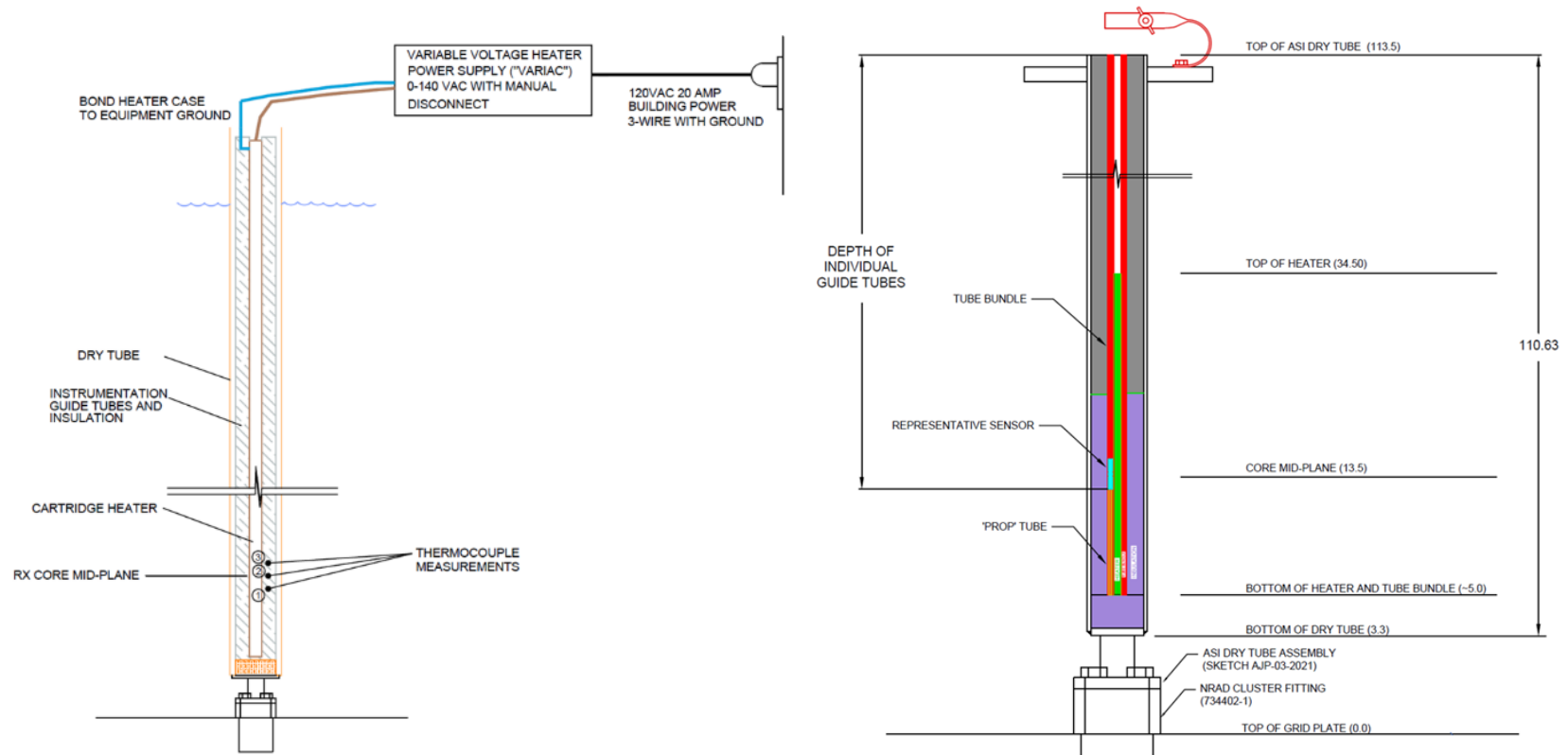


Figure 9. Sideview of NRAD irradiation vehicle. (Left) regarding information on thermocouple and heater configuration. (Right) Assembly height references.

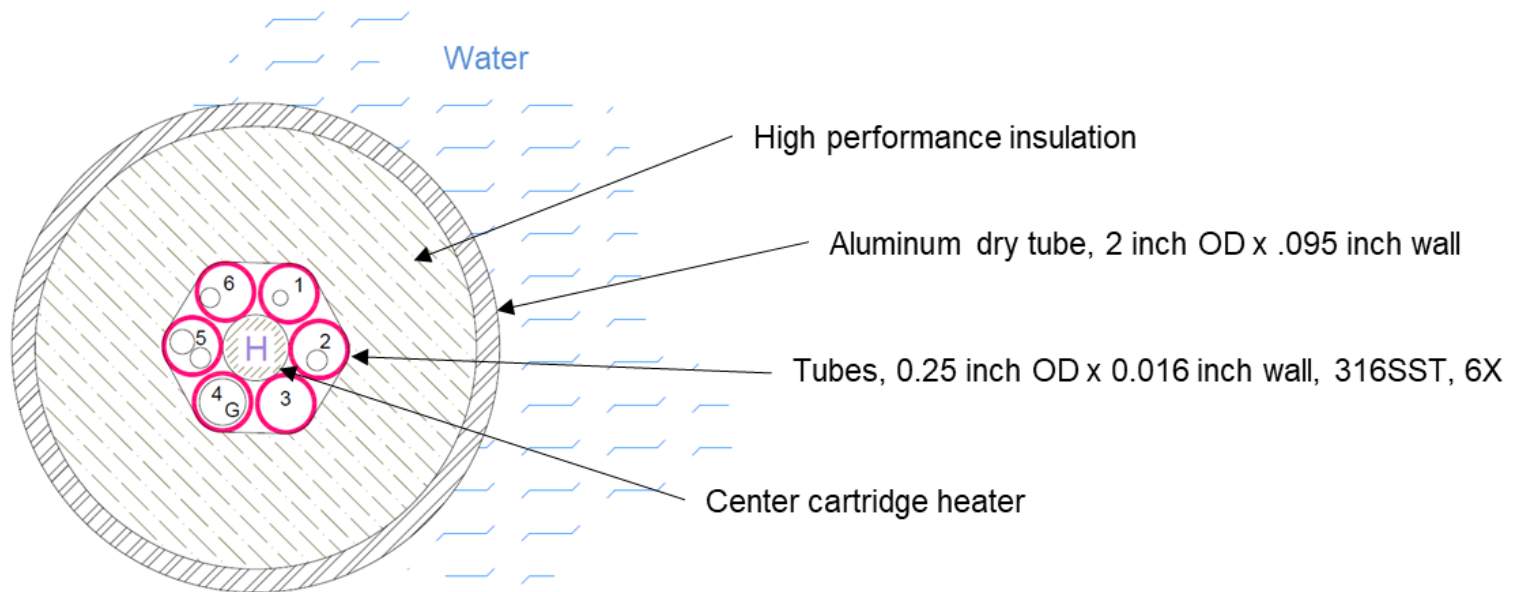


Figure 10. Top-down view of heated irradiation vehicle with sensor position designation numbers.

Table 6. Guide tube depth for each sensor position.

Position	Guide tube depth (in.)	Elevation relative to core mid-plane (in.)
1	101.38	-0.95
2	101.78	-1.35
3	101.66	-1.23
4	102.22	-1.79
5	102.22	-1.79
6	102.22	-1.79

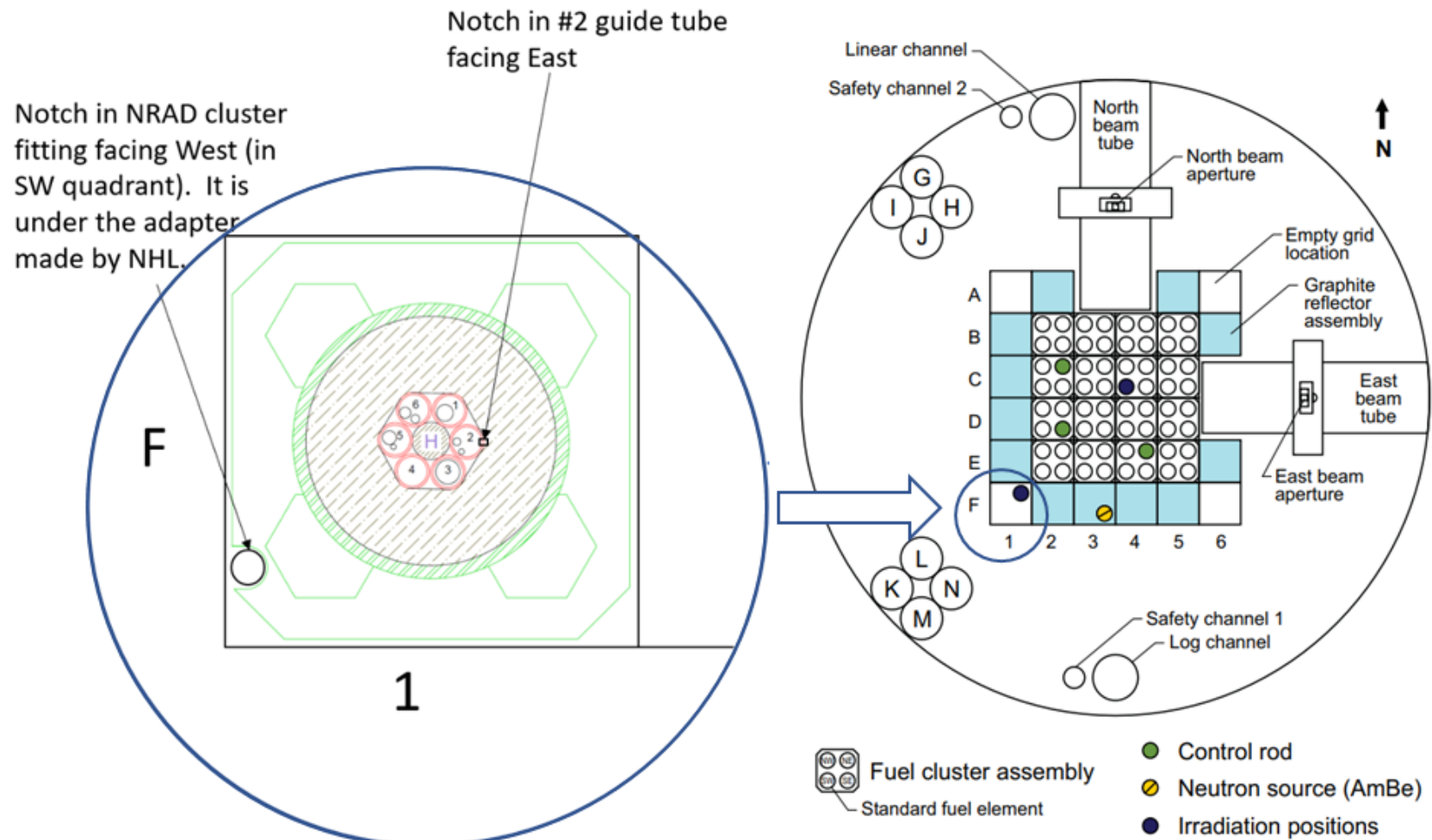


Figure 11. NRAD heated irradiation vehicle orientation and position within the NRAD reactor tank.